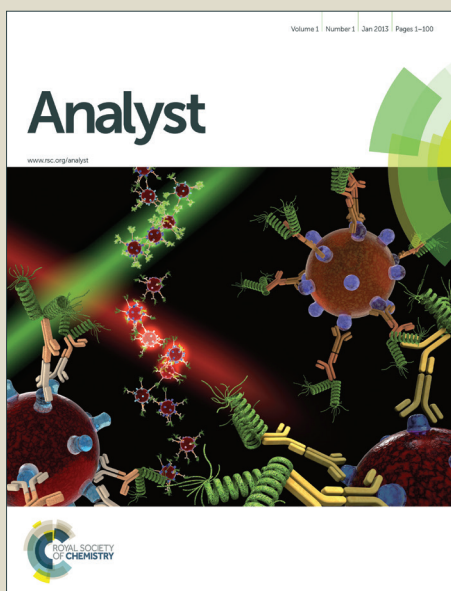


Analyst

Accepted Manuscript



This is an *Accepted Manuscript*, which has been through the Royal Society of Chemistry peer review process and has been accepted for publication.

Accepted Manuscripts are published online shortly after acceptance, before technical editing, formatting and proof reading. Using this free service, authors can make their results available to the community, in citable form, before we publish the edited article. We will replace this *Accepted Manuscript* with the edited and formatted *Advance Article* as soon as it is available.

You can find more information about *Accepted Manuscripts* in the [Information for Authors](#).

Please note that technical editing may introduce minor changes to the text and/or graphics, which may alter content. The journal's standard [Terms & Conditions](#) and the [Ethical guidelines](#) still apply. In no event shall the Royal Society of Chemistry be held responsible for any errors or omissions in this *Accepted Manuscript* or any consequences arising from the use of any information it contains.

Theoretical Analysis of Ion Conductance and Gating Transitions in the OpdK (OccK1) Channel[†]

Karunakar Reddy Pothula and Ulrich Kleinekathöfer^a

Received 5th January 2015, Accepted Xth XXXXXXXXXX 20XX

First published on the web Xth XXXXXXXXXX 200X

DOI: 10.1039/b000000x

Electrophysiological measurements have shown that the channel protein OpdK, also known as OccK1, from *Pseudomonas aeruginosa* shows three conductance substates. Although several experimental studies have been performed, a description of the gating transitions at the molecular level remains elusive. In the present investigation, molecular dynamics simulations have been employed to elucidate the conductance and gating properties of the OpdK channel and loop deletion mutant thereof. Our results suggest that switching between different substates are coupled to conformational changes in the constriction loop L7 which is in accord with the experimental results. Unbiased simulations at different temperatures are analyzed and residues R284 and F291 on loop L7 have been identified to be key in the gating transitions. A plausible mechanism of gating for this channel is discussed. The obtained molecular level description might have important implications for understanding the functional properties of OpdK channel *in vitro* as well as within a cellular environment.

1 Introduction

Membrane proteins are ubiquitous in biological systems and they collectively regulate various transport processes by virtue of their ability to control the passage of ions, nutrients and different substrates across biological membranes¹. Such controlled passage of substrates across channels can be attributed to several properties of membrane proteins, e.g., ion and substrate selectivity as well as gating of the channels. For example, membrane-based ion channels, e.g., potassium channels, allow only a selective passage of certain ions to maintain the necessary electrochemical gradient across the cell membrane which is key to the survival of the cell. Likewise, gating is one of the important mechanisms by which membrane proteins regulate and control the flow of substrates and ions across the membrane. Gating in membrane channels can be mediated via an application of transmembrane voltage, ligand binding or by temperature changes^{1,2}.

Among membrane proteins in the outer membrane of Gram-negative bacteria many β -barrel forming channel proteins are present and especially porins^{3,4}. These channels act as molecular filters and modulate the permeability of the outer membrane by allowing the solutes to pass through them for survival of the cell. In high-resolution time-resolved single channel recordings^{5–9}, membrane pores are often reported to be present in more than one conductance state, e.g., in a high-conducting and a low-conducting state. Various methods

have been employed to understand the gating mechanisms in pore including atomic force microscopy¹⁰, X-ray crystallography¹¹, bilayer electrophysiological measurements^{12,13} and molecular dynamics simulations^{7,14}. However, the exact mechanism by which membrane channels display gating is still not fully understood. Most likely the fluctuations of the pore proteins between different conductance sub-states are the result of local conformational changes induced movements of loops which fold inside the lumen of the pore¹² and/or by a rotational movement of bulky possibly charged residues in the constriction region of the porin⁶.

OpdK, also known as OccK1, is a specific channel belonging to the outer membrane OprD family of *Pseudomonas aeruginosa*. In recent reports, the OprD family is also termed the carboxylate channel (OccK) family according to its substrate specificity¹⁵. The structural features of the substrate specificity of OprD itself were already discussed in 2007¹⁶. Shortly thereafter, the crystal structure of OpdK (OccK1) revealed a monomeric organization of the pore with 18 β strands^{15,17}. The details of the structural features in OpdK channels is discussed elsewhere¹⁷. A clear feature of the channel is that the extracellular loops L3 and L7 fold inside the lumen of the pore forming the constriction region (Fig. 1). Loops L1, L2, L5, L6, L8, L9 are located at the extracellular side of the channel, short in length and have no specific interactions with the residues in the constriction region of the channel. Only loop L4 may indirectly get involved in the dynamics of the constriction region¹⁸. Concerning substrates, the channel favors the uptake of vanillate through the outer membrane¹⁹. Based on electrophysiological experiments it

^a Jacobs University Bremen, Campusring 1, 28759 Bremen, Germany. Fax: +49 421 200 49 3523; Tel: +49 421 200 3523; E-mail: u.kleinekathoef@jacobs-university.de

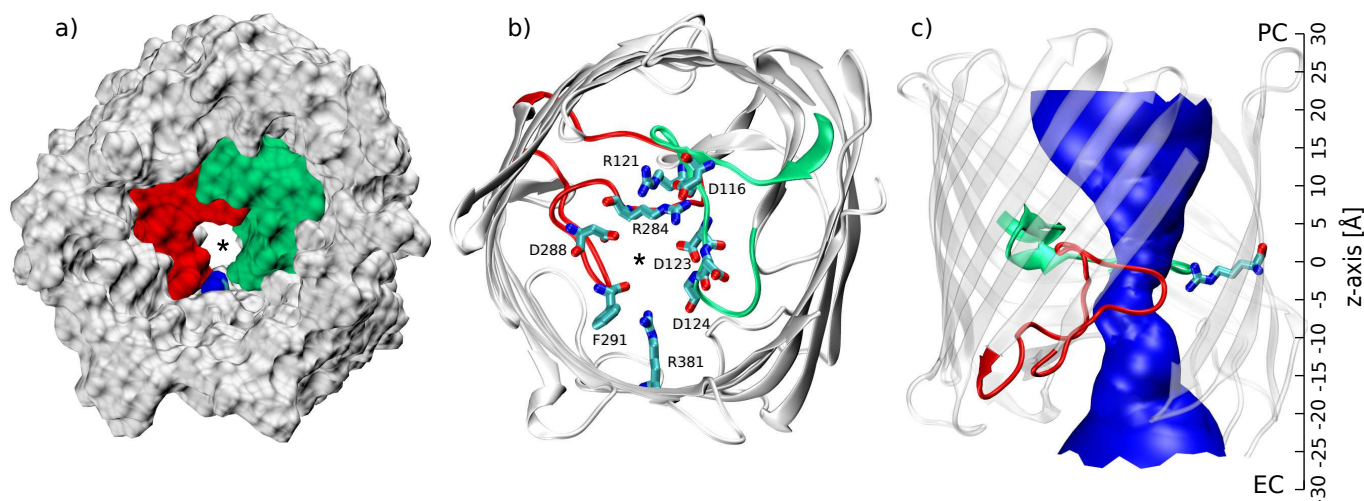


Fig. 1 Structural features of the OpdK channel. a) The constriction region of OpdK is formed by loops L3 and L7. The protein is shown in surface representation highlighting loops L3 and L7 in green and red, respectively. b) Important residues playing a crucial role in the formation of the constriction region are shown in stick representation. The asterisk symbols indicate the approximate position of the channel lumen. c) The pore lumen is shown using a blue surface representation to highlight the relative pore radius in different regions of the channel.

has been reported that OpdK forms a channel with three major conducting states²⁰. However, the nature of the underlying gating mechanism and the transition pathway are unknown. In a series of papers^{5,9,18,20} the subconduction states of OpdK have been detailed with respect to varying transmembrane voltage, ion concentration and temperature. A non-trivial dependence on these parameters has been found and model explanations have been provided. In the present study we investigate the molecular basis for the gating behavior of the OpdK channel using all-atom molecular dynamics simulations (MD) to obtain a molecular-level description of the underlying mechanisms.

Computational MD simulations can provide atomic-level information on many biological processes and can effectively complement electrophysiological bilayer measurements^{21,22}. Previously, MD simulations have been used to study the dynamics of various bacterial pores such as the porin pore²³, MscS²⁴, α -hemolysin²⁵, OmpG⁷, OmpA¹⁴, OmpF^{26,27}, OmpC²⁸, FecA²⁹, OprP^{30–32}, OprD^{33,34}, and others. However, it is computationally challenging to model gating processes due to the long timescale associated with such processes^{7,14}. Nevertheless, several non-equilibrium MD approaches are available which can accelerate the motions of proteins and make them accessible to the time-scales associated with MD simulations. We want to emphasize that one important reason for studying the transport and gating properties of bacterial membrane pores is their function as channel for antibiotics. This topic is beyond the scope of the present investigation but is actively being studied, e.g., employing molecular simulations^{35–39}.

2 Materials and Methods

In this study, we have performed MD simulations on three systems, the native OpdK channel and two loop-deletion mutants, i.e., OpdK- Δ L3 and OpdK- Δ L7. Below the systems are detailed together with the corresponding MD simulations.

2.1 System setups

The crystal structure of the OpdK channel (PDB ID: 3SYS)¹⁵ was employed as starting structure. The missing loops residues (loop L1: 25–32, loop L2: 72–75) were modeled using the structure of a BenF-like porin (PDB ID: 3JTY)⁴⁰ using the software MODELLER⁴¹. These loops L1 and L2 are short and have no direct interaction with loops L3 and L7. Subsequently, two OpdK mutants, i.e., OpdK- Δ L3 and OpdK- Δ L7, were prepared from the starting structure using MODELLER. The loop deletions were selected according to the earlier experimental studies^{5,9}. Moreover, the OpdK channel was embedded into a POPE lipid bilayer which was constructed from pre-equilibrated patches using VMD⁴². To this end, the membrane was aligned parallel to the xy plane and centered in the z direction. A 1 M KCl solution was added using the TIP3P water model. For the OpdK- Δ L3 and OpdK- Δ L7 mutants the systems were prepared likewise. Some more details of the systems are given in the Table 1.

2.2 MD simulations

The above described systems have been simulated under equilibrium and nonequilibrium conditions. In nonequilibrium

Table 1 Summary of the system properties and MD simulations performed on OpdK and its mutants.

Sl.no	Channel	Residue index of deletion	No of residues deleted	Temperature [K]	Concentration [M]	Type of simulation	Length [ns]
1	OpdK	-	-	310	1	unbiased MD	50
2	OpdK	-	-	330	1	unbiased MD	50
3	OpdK	-	-	350	1	unbiased MD	50
4	OpdK	-	-	370	1	unbiased MD	50
5	OpdK	-	-	310	1	applied-field MD	50
5	OpdK- Δ L3	124 to 129	6	310	1	unbiased MD	50
6	OpdK- Δ L3	124 to 129	6	310	1	applied-field MD	50
7	OpdK- Δ L7	281 to 287	7	310	1	unbiased MD	50
8	OpdK- Δ L7	281 to 287	7	310	1	applied-field MD	50

simulations, a constant voltage of 1.0 V was applied whereas the equilibrium simulations were performed in the absence of any external bias as summarized in Table 1. The bias was implemented by applying a constant uniform electric field E along the z direction. This results in a voltage $V = E \cdot L_z$ with L_z being the length of the periodic cell in z direction. This method has been widely adopted to achieve a transmembrane potential in MD simulations^{25,43}. We note that throughout this study, a high electrostatic potential is defined as the periplasmic side of the membrane and a lower potential at the extracellular side of the membrane such that the resulting electric field is directed towards negative $-z$ values.

All MD simulations were performed using the program NAMD 2.9⁴⁴ and the CHARMM27 force field⁴⁵. As in most MD simulations, periodic boundary conditions were applied in the simulations. The temperature was maintained by Langevin dynamics acting only on the heavy atoms of the lipids with a damping constant of 1.0 ps^{-1} . Long-range electrostatic interactions were determined using the particle mesh Ewald method⁴⁶ whereas short-range non bonded interactions using a cutoff of 12 \AA and a switching distance of 10 \AA . Employing the r-RESPA multiple time step method⁴⁷, bonded interactions have been evaluated every 2 fs while short-range nonbonded and long-range electrostatic interactions every 2 fs and 4 fs, respectively. Bond constraints were applied to hydrogen atoms applying the SHAKE algorithm⁴⁸. The system was equilibrated for 5 ns in an NPT ensemble followed by a 5 ns equilibration run in an NVT ensemble. Finally, production runs with and without applying an external electric field were performed in an NVT ensemble and details of the simulations are shown in the Table 1.

2.3 Ion conductance calculations

Analyzing the applied field simulations, the instantaneous current at time t can be determined using²⁵

$$I(t) = \frac{1}{L_z \Delta t} \sum_i^N q_i \Delta z_i \quad (1)$$

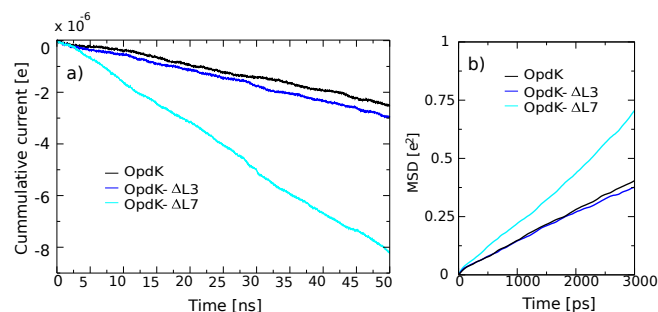


Fig. 2 a) Cumulative currents obtained from the non-equilibrium MD simulations. b) Mean-squared displacements (MSDs) calculated from the equilibrium trajectories of OpdK channel and its mutants. Linear fits for extracting the slope have been performed using the data between $t = 2000$ ps and $t = 3000$ ps.

where q_i is the charge of atom i and Δz_i the displacement of atom i during Δt . The K^+ and Cl^- currents can be determined separately and then combined to yield the net ionic currents. To this end, the cumulative currents can be obtained by adding up the instantaneous currents at every sampling time^{25,27}. A linear fit of this cumulative current versus time leads to the average current. Subsequently, the conductance can be obtained as ratio of ionic current and applied voltage.

As an alternative approach, we employ the collective diffusion model developed by Liu and Zhu⁴⁹. This model is based on an unbiased MD simulation together with linear response theory. One first needs to determine the average total charge movement and at the same time the amount of transferred charge. Within linear response theory, these quantities are then combined to obtain the conductance. For some test cases and small voltages, this approach has been shown to yield the same results as the above applied-field simulations though more efficiently⁴⁹.

Table 2 Theoretical conductances (in units of pS) determined from equilibrium and non-equilibrium MD simulations. In addition, the ratio to the respective wild type value is given.

Channel	Applied Field Simulations		Collective Diffusion Model		Experimental Conductance ⁵	
	conductance	ratio to wt	conductance	ratio to wt	conductance	ratio to wt
OpdK	498	1	348	1	307 ± 14 pS	1
OpdK-ΔL3	583	1.17	319	0.91	~ 300	0.98
OpdK-ΔL7	1692	3.39	697	2.00	~725	2.36

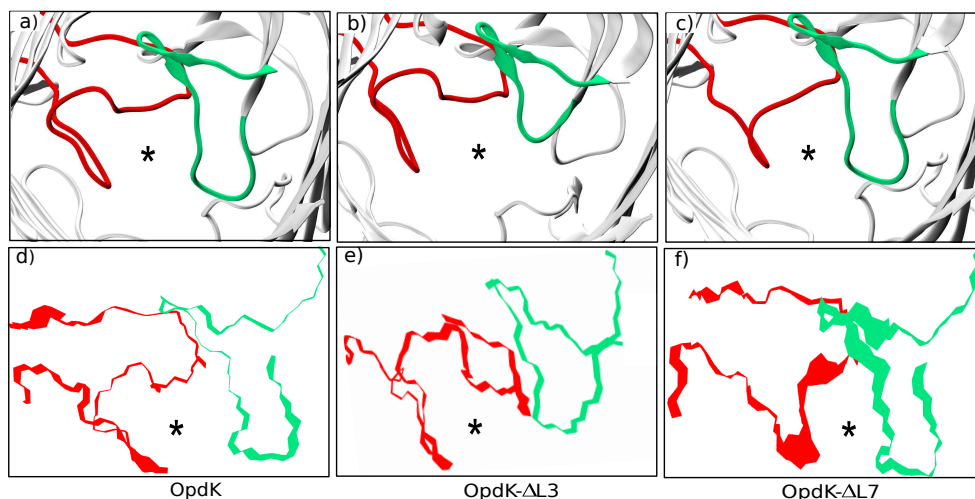


Fig. 3 Comparison of the OpdK and its mutant trajectories obtained from equilibrium MD simulations. Panels a-c: Visualization of the constriction region of OpdK channel and its mutants. Panels d-f: The superimposed conformations of the loops L3 (green) and L7 (red) of OpdK and its mutant shown in line presentation. The conformational fluctuations are filtered along the first principal component. The asterisk symbols indicate the approximate positions of the channel lumen.

3 Simulations of Ion Conductance

Experimental studies^{5,9,18,20} on the OpdK channel revealed that the channel exists in three major distinct conformations: a dominant O2 substate with a conductance of 307 ± 14 pS, a state O3 with the second highest probability and the largest conductance of 357 ± 24 pS and a state O1 with a relative low probability and a conductance of 223 ± 50 pS²⁰. Though details vary, this kind of gating behavior is seen independent of salt concentration and applied voltage⁹.

Cheneke et al.⁵ experimentally studied different loop deletions to understand the dynamics of the single channel current fluctuations exhibited by the native OpdK channel. In the present study we follow the same route to complement the electrophysiological observations with atomic-level details from simulations. As shown in Fig. 1, the two extracellular loops L3 and L7 fold into the lumen of the channel and structure the constriction region. In order to investigate the effects of the loops L3 and L7, mutants were produced and electrophysiologically characterized. To this end, fragments of the loops were selected that expose to the lumen of the channel. Furthermore, the residues immediately before and

after the deletion needed to be close enough in space so that they can be replaced by a single glycine residue without introducing significant conformational changes in the channel. So for the purpose of studying the loop effects, the mutant OpdK-ΔL3 was produced from wild type OpdK by deleting residues Asp124 to Pro129 on loop L3 and mutant OpdK-ΔL7 by removing Ser281 to Gly287 on loop L7⁹.

The same mutants were produced *in silico* and subsequently the conductances for the OpdK as well as the OpdK-ΔL3 and OpdK-ΔL7 mutants channels were determined. These results are based on non-equilibrium simulations applying a constant voltage^{25,26,43} but also on equilibrium MD simulations using the collective diffusion model⁴⁹. Shown in Fig. 2 are the cumulative currents for the simulations with +1V applied. From the slope of these curves the current can be extracted. The calculated conductance values of the native and mutant channels in the 1M KCl solution are listed in Table 2. For the applied field simulations at 1 V, one could only expect to obtain a good agreement with experiment if the current-voltage relation would be linear which is very unlikely for such a narrow pore. At the same time, the ratios of conductance between mutant and wild type channel are in quite reasonable agree-

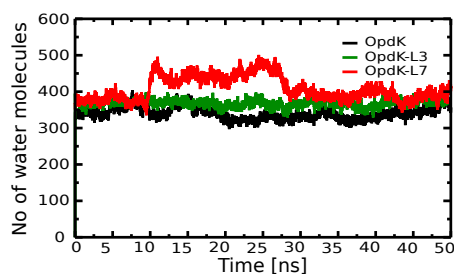


Fig. 4 Change in the water filling in the channels. The water molecules in the range from -15\AA to $+15\text{\AA}$ are counted for this measure.

ment with those from experiment. This finding indicates that applied-field simulations even at higher voltages can indeed be helpful in understanding molecular properties of conductance. We note in passing that we did not include selectivity data from the simulations since single permeating ions can lead to large fluctuations in the selectivity of a narrow channel like OpdK.

Using the collective diffusion model by Liu and Zhu⁴⁹ the conductance within the linear response regime, i.e., for small bias voltages, can be extracted from equilibrium simulations. The corresponding values are much closer to the experimental values than applied field results at an applied voltage of 1 V. Again the ratios of conductance of mutant and wild type channels agree even better. Both in theory and experiment, the conductance of the OpdK- Δ L3 mutant is very similar to that of the native protein. In contrast, a high increase in conductance can be seen for the OpdK- Δ L7 mutant. The conductance for this mutant is more than double than that of the native OpdK channel in good agreement between theory and experiment.

Furthermore, we compared the dynamics of the native OpdK pore with its OpdK- Δ L3 and OpdK- Δ L7 mutants to complement the electrophysiological observations with atomic-level details. Equilibrium trajectories of OpdK and its mutants at 310K were used to analyze the differences in the dynamics. Figures 3a-c visualize the mutants while panels a-f show the superimposed conformations of OpdK and its mutants filtered along the first eigenvector reflecting the deviations of the C_{α} atoms of the loops aligned to the initial structure. This principal component analysis (PCA) which splits the complex dynamics into a few principal modes helps to explain the major movements observed during the MD. In addition to the PCA analysis, the number of water molecules in the channel has been analyzed to indirectly assess the cross-section area of the channels (see Fig. 4). The deletion of the D124-P129 fragment did not alter the dynamics of loop Δ L3 or L7 in OpdK- Δ L3 channel. Overall, in the simulations the mutant OpdK- Δ L3 has shown no significantly different behavior compared to the wide type. Likewise, experimental studies

of the OpdK- Δ L3 mutant found similar single-channel electrical recordings consisting of three major open states⁹. This suggests that the residues D124-P129 in OpdK channel neither have an active role in gating nor do they influence the residues involved in the gating process. These findings are different for the OpdK- Δ L7 mutant which appears to be consistent with the single channel measurements on the OpdK- Δ L7 channel. This mutant pore has shown large and rapid fluctuations in single channel current recordings⁹. As shown in the Fig. 3, the Δ L7 loop in the OpdK- Δ L7 mutant fluctuates much more due to the lack of the D116-R284 salt bridge. Thus, the pore size of the OpdK- Δ L7 channel can vary much more (consistent with Fig. 4) compared to the OpdK and OpdK- Δ L3 pores. This fact leads to an increased conductance by nearly a factor of two in experiments and theoretical calculations. In addition to experiments, our MD results also support the role of loop L7 in gating. The dynamics of loops L3 and L7 will be compare in more detail below.

4 Molecular Determinants of Gating Transitions

4.1 Is loop L3 or L7 more flexible?

Usually flexible parts in the lumen of a channel are responsible for gating phenomena. For instance, the constriction loop in OmpC has been suggested to be important in the gating process^{12,50}. Correspondingly, in OpdK the loops L3 or L7 are likely very important for the multiple substates. Hence, we have performed a structural analysis of these loops and compared their flexibility. To this end, we performed molecular dynamics simulations of the OpdK channel at various temperatures as shown in Table 1.

The analysis of the root mean square deviation (RMSD) shows that the flexibility of loop L7 is higher than that L3 at any particular simulation temperature and increases with rise in the temperature as shown in Figs. 5a-d. Loop L3 does not shown much variation in the RMSD values and remains rigid even at higher temperatures. In addition, we analyzed the equilibrium trajectories of OpdK channel at different temperatures again employing a PCA analysis. Here we described the dynamical differences in the loops L3 and L7 of the OpdK channel along the first eigenvector which account for the major motion of the channel. Figures 5e-h show the superimposed conformations at different temperatures filtered along the first two eigenvectors which reflects the deviation of the C_{α} atoms with respect to the initial structure. In each case, the motion is dominated by loop L7. From this analysis, it is clearly evident that the L7 residues deviate more than the L3 ones from the initial structure. Therefore, loop L7 is found to be more flexible than L3.

The conformational rigidity of loop L3 can be attributed to

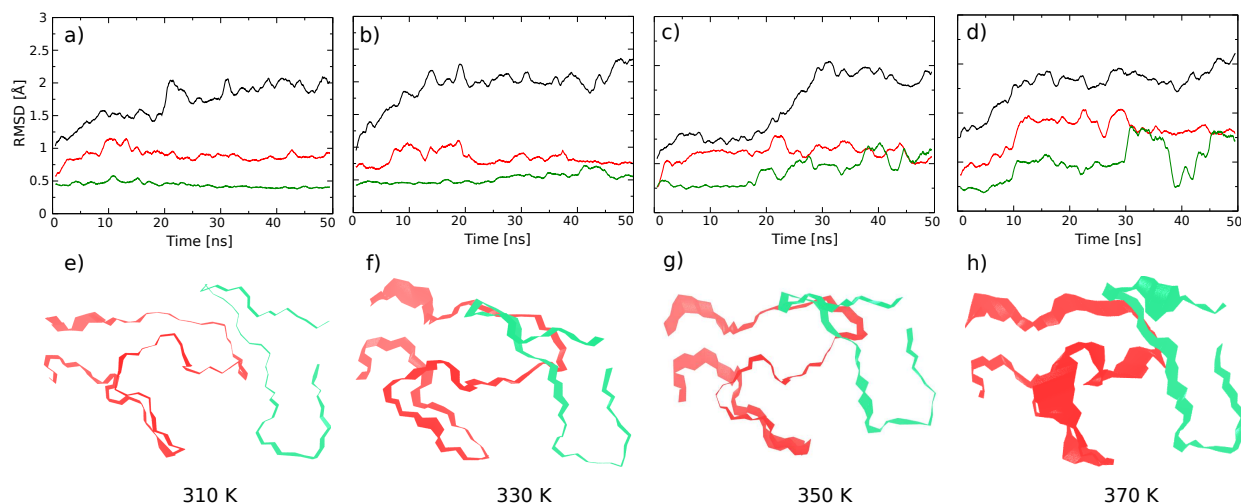


Fig. 5 Comparison of the OpdK trajectories obtained from equilibrium MD simulations at various temperatures. Panels a-d: RMSD values of the C_{α} atoms of the protein (black) and the loops L3 (green) as well as L7 (red) at 310 K, 330 K, 350 K, and 370 K. Panels e-h: The corresponding superimposed conformations of the loops L3 (green) and L7 (red) in line presentation. Shown are conformational changes filtered along the first principal component.

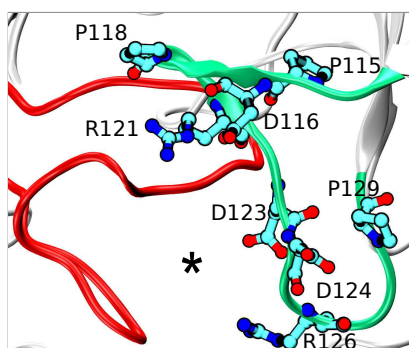


Fig. 6 Visualization of the proline and charged residues present in loop L3. The protein is shown in cartoon (loops L3 in green and L7 in red) and the residues in stick representation.

two structural features. This loop has three proline residues (see Fig. 6) which sterically hinder its movement. As a second point, L3 loop contains more charged residues than L7 and these charged entities form salt-bridges or electrostatic connections and therefore become more rigid. A sequence analysis of OpdK and the other members of its family shows that the L3 loop contains conserved proline residues (data not shown here). Due to the presence of the cyclic side chain in the proline residues, the corresponding peptide bond has fewer possibilities of rotation and therefore, it imparts rigidity in L3.

Overall, loop L7 is found to be more flexible compared to loop L3 and appears to play a main role in gating. As already mentioned, recent electrophysiological studies showed that loop L7 deletion has a clear effect on the conductance

and gating behavior of the pore⁹. The L3 deletion mutant of OpdK, in contrast, showed a behavior similar to that of the native protein. For this reason we focus our molecular-level analysis on the significance of loop L7 in gating.

4.2 Prominent local conformational changes observed in MD simulations

In a next step we turn to discuss the local conformational changes occurring during the MD simulations. Note that because of the finite length of the simulations one has to be very careful concerning statements based on single trajectories. To improve the sampling of the various protein conformations, we analyzed simulations at different temperatures (310 K, 330 K, 350 K, and 370 K). Certainly this is only a rough but also quite efficient way to enhance the sampling. In the analysis of the resulting trajectories we looked for common patterns to ensure the validity of our statements. Visual inspection of representative structures at each temperature indicate small and local structural changes in the lumen of the channel. Indeed, the OpdK substates have conductances in the same order of magnitude indicating the role of local rather than global conformational changes during the gating transition.

Furthermore, we calculated the inter-residue distances F291-G125 and R284-R381 (Fig. 7a) to quantify the conformational changes in the constriction region. As shown in Fig. 7b, the F291-G125 distance is reduced at all simulated temperatures due to the flipping of the aromatic ring of the F291 residue towards the lumen of the channel. Likewise, the R284-R381 distance was reduced (Fig. 7c) as result of the

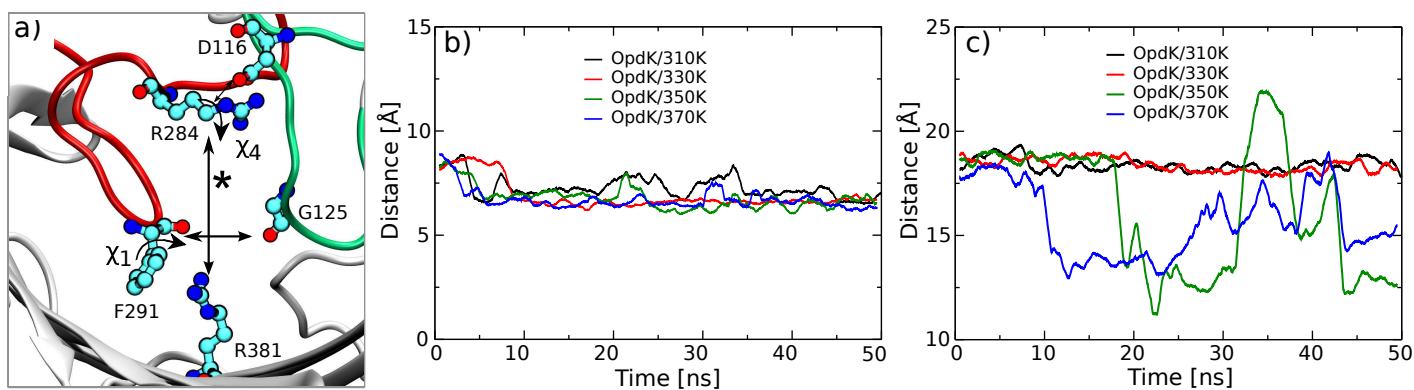


Fig. 7 Change in the structural properties of OpdK channel from trajectories of unbiased simulations at different temperatures (a) Calculated structural properties, e.g., χ_4 dihedral angle of R284, χ_1 dihedral angle of F291 and inter residue distances F291-G125 and R284-R381 are shown. Change in the distance between the residues during the course of the simulations (b) F291(CG) - G125(CA) (c) R284(CZ) - R381(CA).

movement of R284 residue towards the lumen of the channel after breaking the salt-bridge with the residue D116 on loop L3. However, this distance was changed only at high temperatures (350K and 370K) due to the presence of a salt-bridge between R284 and D116 residue. The conformational changes of residues F291 and R284 in the constriction region can be discussed by looking at the dihedral angles of the side chains. Fig. 8 shows the dihedral angles of the F291 and R284 residues along the trajectories. F291 can adopt two different rotameric states, i.e., χ_1 approximately 60° or approximately 120° . Also R284 can assume two different rotameric states with χ_4 approximately 60° or 180° but only at high temperatures after the breaking the electrostatic interaction with D116. These two residues, F291 and R284, have a high degree of freedom due to the rather extended side chains and at the same time are positioned at different locations on the loop L7 in the constriction region. From the electrophysiological studies it is clear that no direct transition occurs between the substates O1 and O3. This finding indicates that the O1 \leftrightarrow O2 and O2 \leftrightarrow O3 transitions represent the conformational changes of independent parts in the lumen of the channel⁹. This argument supports the two observed conformational changes found in the MD simulations.

It has been reported⁵ that applied transmembrane voltages show an effect on the kinetic rate constants of the O2 to O1 transition and not on the O2 to O3 transition. This finding suggests that charged residue might be participating in the O2 to O1 transition and is fully in accord with the positively charged R284 residue found in our MD simulations. In addition, it is concluded from the experiments that the barrier for crossing from the O2 to the O1 state is higher than that from O2 to O3. Furthermore, the change in enthalpy ΔH for moving from substate O1 to O2 is negative which suggest a decrease in loop flexibility and formation of intramolecular bond^{5,9,18}. This observation also appears to consistent with

the R284 residue which shows a electrostatic interaction with D116. Upon switching from the O2 to the O1 substate, the R284 residue breaks the salt-bridge with D116 and moves towards the lumen of the channel or vice versa.

On the other hand, the O2 to O3 transition frequency increases with elevating the temperatures and has no influence on the kinetics at different applied voltages. We envision that the fluctuations of the hydrophobic residue F291 trigger the O2 to O3 transition. The aromatic ring of the F291 residue is flexible and can flip towards the lumen of the channel at all temperatures in our simulations. Overall, our observed conformational changes are consistent with the experimental findings^{5,9,18}.

4.3 Plausible mechanism of gating

As mentioned earlier, single channel recordings have shown that a dominant state of the OpdK is the high conducting O2 substate⁹. Hence, it is fair to assume that the crystal structure of this pore also showing this dominant O2 state. Here, we discuss the mechanism of gating based on the example trajectory of the OpdK channel at 370 K. During the gating transition from the O2 to the O3 substate, the phenylalanine, F291, present in loop L7, changes its rotameric state and moves towards loop L3. This change in the rotameric state as highlighted in Fig. 9 (middle to left panel) can be quantified by performing an analysis of the dihedral angle belonging to the corresponding side chain of the residue. As shown in Fig. 10a the side chain dihedral angle of F291 (χ_1) changes from about 60° to roughly 180° .

The gating transition from the O2 to the O1 substate involves breaking an electrostatic interaction between the loops L3 and L7. In addition, the bulky positively charged residue R284 changes its conformation after breaking a salt bridge with D116 residue and moves towards the lumen of the chan-

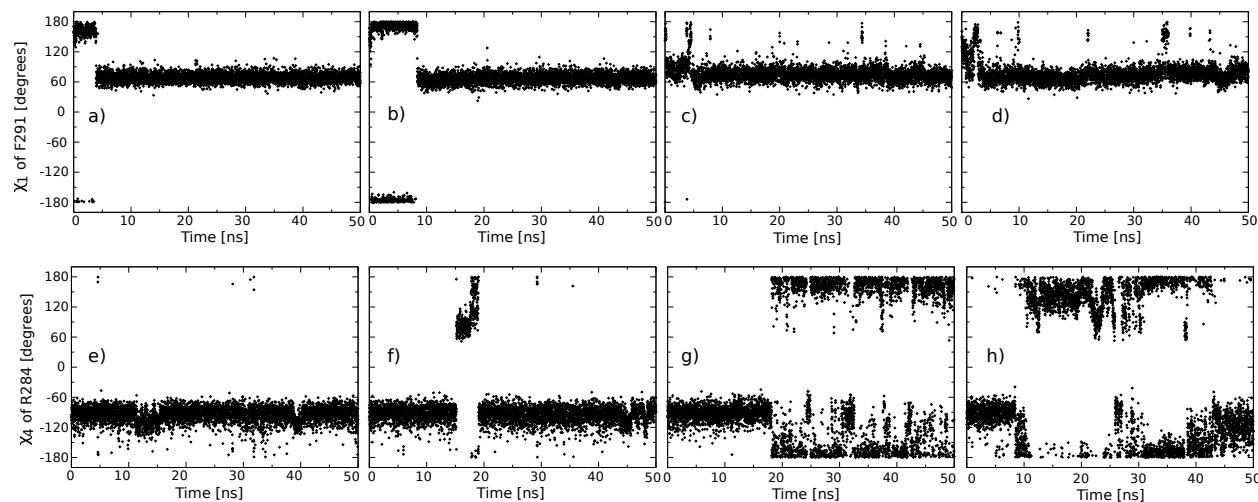


Fig. 8 Comparison of the side chain angle dynamics of the residues F291 (panels a-d) and R284 (panels e-h) residues at different temperatures.

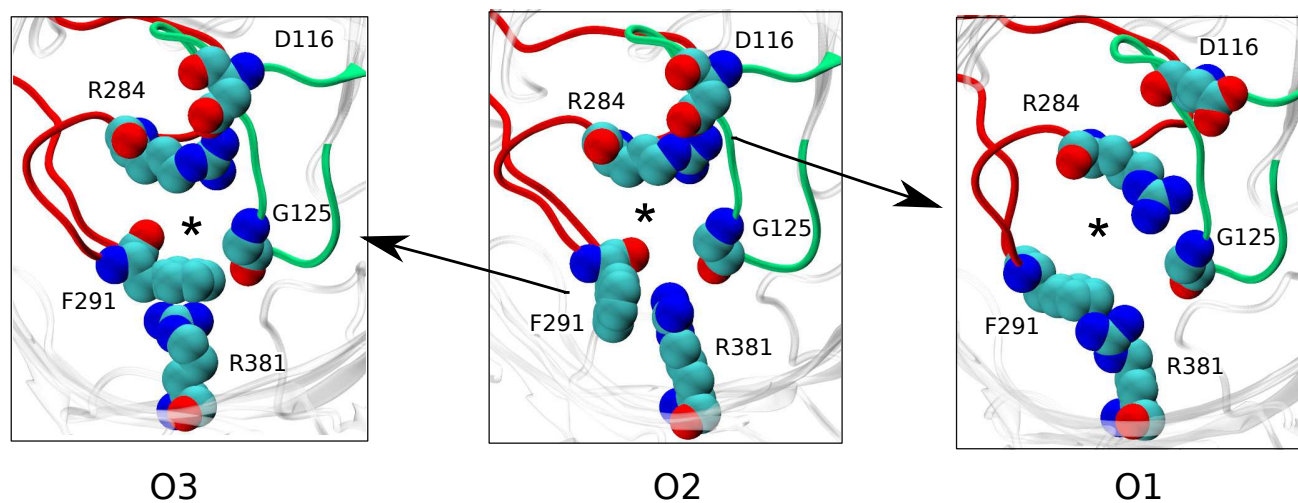


Fig. 9 Possible mechanism for the gating transition from state O2 to O3 and from state O2 to O1 state in the OpdK channel. Loop L7 (red), L3 (green) and important residues (shown in van der Waals representation) which form the constriction region are emphasized. The asterisk symbol indicates the approximate position of the channel lumen.

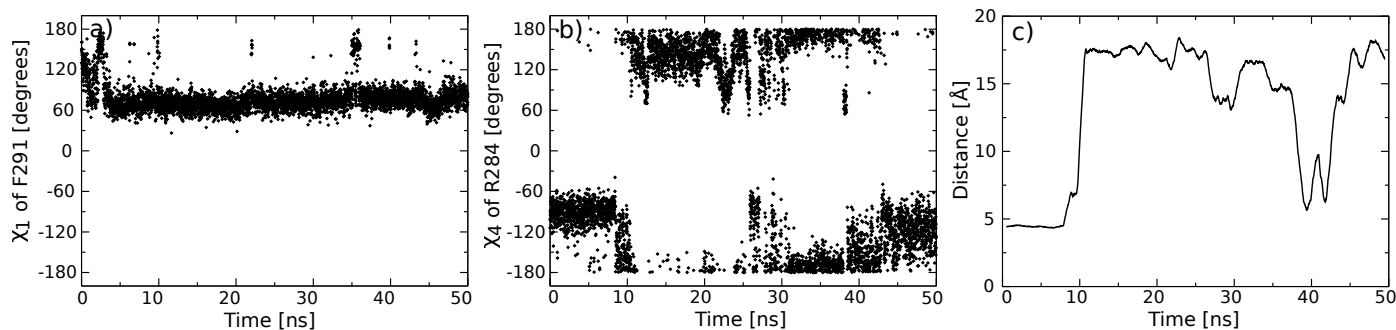


Fig. 10 Change in structural properties of the OpdK channel during gating transitions from the O2 to the O3 substate and from the O2 to the O1 substate as observed in unbiased simulations at 370K. a) Change in the dihedral angle (χ_1) of the F291 side chain during the simulation. b) Change in the dihedral angle (χ_4) of the R284 side chain during the transition from the O2 to the O1 substate. c) Distance between residues R284 and D116 involved in the salt bridge between loops L3 and L7.

nel. Contributions of a charged and bulky residue like arginine to the gating process by virtue of its ability to form salt-bridges and acquiring different side chain conformations have been reported already for the porin OmpA¹⁴. The change in the salt bridge between R284 and D116 is shown in the transition from the middle to the right panel in Fig. 9. It can be quantified by the distance between these two residues as shown in Fig. 10c. In addition, the change in the R284 side chain conformation (χ_4) during the transition from the O2 to the O1 substate is depicted in Fig. 10b.

Our results strongly indicate that the presence of the loops in the constriction region, particularly of loop L7, along with their interplay with bulky residues (R282 and F291 in OpdK) play a crucial role in defining different conductance substates of the channels belonging to the OpdK family. Recently, the importance of loop L7 in the dynamics of the OprD channel, a homologue of OpdK, is discussed from MD simulations³³.

The role of loops, which fold inside the lumen of the channel, in assigning different conductance substates has previously been reported for porins like OmpF and OmpC from *E. coli*^{13,28,50}.

5 Conclusions

In this study, MD simulations have been carried out to investigate the conformational changes in the channel OpdK. OpdK is a specific pore present in the outer membrane of Gram-negative bacteria *P. aeruginosa*. Previous electrophysiological studies^{5,9,18,20} have shown OpdK channel to exist in three distinct substates, named as O1, O2 and O3.

We performed unbiased simulations at different temperatures in order to enhance the molecular level understanding behind these conductance and gating properties. The side chain dynamics of the residues F291 and R284 of loop L7 has been found to influence the dimensions of the constriction

zone. The hypothesis coming out of these simulation is that the transition between the substates can qualitatively be described using the dihedral angles of the side chains belonging to residues F291 and R284.

Based on our results, a plausible mechanism of channel gating is suggested in Fig. 9. All observed conformational changes are quite local but, nevertheless, relevant to the conducting states reported for the OpdK channel. This proposed gating mechanism has to be tested experimentally by performing site directed mutagenesis. The work presented here supports the idea that loop L7 and its bulky residues F291 and R284 play a key role in switching to different conformational substates. The hypothesis of loop L7 involvement in the dynamics is consistent with a recent electrophysiological study on the OpdK channel⁵. It needs to be seen in how much this finding is also a feature in the other channels of the OpdK family and, at this moment of time, we cannot completely rule out that additional parts of the protein play a role in the experimentally observed gating. For example, a possible indirect effect of loop L4 on the dynamics of the constriction region might need to be taken into account¹⁸. Further investigations in this direction are in progress. Moreover, the behavior of the OpdK channel in more realistic LPS containing outer membranes should be investigated. These simulations are now possible since LPS-containing outer membrane models of Gram-negative bacteria have recently been reported^{29,51}.

Acknowledgments

The research leading to the results discussed here was conducted as part of the Translocation consortium (www.translocation.eu) and has received support from the Innovative Medicines Joint Undertaking under Grant Agreement No. 115525, resources which are composed of financial contribution from the European Union's sev-

enth framework programme (FP7/2007-2013) and EFPIA companies in kind contribution.

References

- 1 Bertil Hille, *Ion Channels of Excitable Membranes*, Sinauer, Sunderland, MA, 3rd edn, 2001.
- 2 M. R. Blatt and G. Thiel, *Annu. Rev. Plant Biol.*, 1993, **44**, 543–567.
- 3 H. Nikaido, *Microbiol. Mol. Biol. Rev.*, 2003, **67**, 593–656.
- 4 *Bacterial and Eukaryotic Porins*, ed. R. Benz, Wiley-VCH, Weinheim, 2004.
- 5 B. R. Cheneke, B. van den Berg and L. Movileanu, *Biochemistry*, 2011, **50**, 4987–4997.
- 6 H. Hong, G. Szabo and L. K. Tamm, *Nat. Chem. Biol.*, 2006, **2**, 627–635.
- 7 M. Chen, S. Khalid, M. S. P. Sansom and H. Bayley, *Proc. Natl. Acad. Sci. USA*, 2008, **105**, 6272–6277.
- 8 W. L. Hwang, M. Chen, B. Cronin, M. A. Holden and H. Bayley, *J. Am. Chem. Soc.*, 2008, **130**, 5878–5879.
- 9 B. R. Cheneke, M. Indic, B. van den Berg and L. Movileanu, *Biochemistry*, 2012, **51**, 5348–5358.
- 10 S. A. Mari, S. Köster, C. A. Bippes, Ö. Yildiz, W. Kühlbrandt and D. J. Muller, *J. Mol. Biol.*, 2010, **396**, 610–616.
- 11 B. W. Lepore, M. Indic, H. Pham, E. M. Hearn, D. R. Patel and B. van den Berg, *Proc. Natl. Acad. Sci. U. S. A.*, 2011, **108**, 10121–10126.
- 12 N. Liu, H. Samartzidou, K. W. Lee, J. M. Briggs and A. H. Delcour, *Protein. Eng.*, 2000, **13**, 491–500.
- 13 A. Basle, R. Iyer and A. H. Delcour, *Biochim. Biophys. Acta*, 2004, **1664**, 100–107.
- 14 S. Khalid, P. J. Bond, T. Carpenter and M. S. Sansom, *Biochimica et Biophysica Acta (BBA)-Biomembranes*, 2008, **1778**, 1871–1880.
- 15 E. Eren, J. Vijayaraghavan, J. Liu, B. R. Cheneke, D. S. Touw, B. W. Lepore, M. Indic, L. Movileanu and B. van den Berg, *PLoS Biol.*, 2012, **10**, e1001242.
- 16 S. Biswas, M. M. Mohammad, D. R. Patel, L. Movileanu and B. van den Berg, *Nat. Struct. Mol. Biol.*, 2007, **14**, 1108–1109.
- 17 S. Biswas, M. M. Mohammad, D. R. Patel, L. Movileanu and B. van den Berg, *Structure*, 2008, **16**, 1027–1035.
- 18 B. R. Cheneke, B. van den Berg and L. Movileanu, *ACS Chem. Biol.*, 2014, (in press).
- 19 S. Tamber, E. Maier, R. Benz and R. E. W. Hancock, *J. Bacteriol.*, 2007, **189**, 929–939.
- 20 J. Liu, E. Eren, J. Vijayaraghavan, B. R. Cheneke, M. Indic, B. van den Berg and L. Movileanu, *Biochemistry*, 2012, **51**, 2319–2330.
- 21 N. Modi, M. Winterhalter and U. Kleinekathöfer, *Nanoscale*, 2012, **4**, 6166–6180.
- 22 C. Maffeo, S. Bhattacharya, J. Yoo, D. Wells and A. Aksimentiev, *Chem. Rev.*, 2012, **112**, 6250–6284.
- 23 C. Soares, J. Björkstén and O. Tapia, *Protein Eng.*, 1995, **8**, 5–12.
- 24 M. Sotomayor and K. Schulten, *Biophys. J.*, 2004, **87**, 3050–3055.
- 25 A. Aksimentiev and K. Schulten, *Biophys. J.*, 2005, **88**, 3745–3761.
- 26 C. Chimere, L. Movileanu, S. Pezeshki, M. Winterhalter and U. Kleinekathöfer, *Eur. Biophys. J.*, 2008, **38**, 121–125.
- 27 S. Pezeshki, C. Chimere, A. Bessenov, M. Winterhalter and U. Kleinekathöfer, *Biophys. J.*, 2009, **97**, 1898–1906.
- 28 I. Biro, S. Pezeshki, H. Weingart, M. Winterhalter and U. Kleinekathöfer, *Biophys. J.*, 2010, **98**, 1830–1839.
- 29 T. J. Piggot, D. A. Holdbrook and S. Khalid, *Biochimica et Biophysica Acta (BBA) - Biomembranes*, 2013, **1828**, 284–293.
- 30 N. Modi, R. Benz, R. E. W. Hancock and U. Kleinekathöfer, *J. Phys. Chem. Lett.*, 2012, **3**, 3639–3645.
- 31 N. Modi, I. Bárcena-Urbarri, M. Bains, R. Benz, R. E. Hancock and U. Kleinekathöfer, *Biochemistry*, 2013, **52**, 5522–5532.
- 32 N. Modi, I. Bárcena-Urbarri, M. Bains, R. Benz, R. E. Hancock and U. Kleinekathöfer, *ACS Chem. Biol.*, 2015, **10**, 441–451.
- 33 E. Eren, J. Parkin, A. Adelanwa, B. Cheneke, L. Movileanu, S. Khalid and B. Van den Berg, *J. Biol. Chem.*, 2013, **288**, 12042–12053.
- 34 J. Parkin and S. Khalid, *Biophys. J.*, 2014, **107**, 1853–1861.
- 35 C. Danelon, E. M. Nestorovich, M. Winterhalter, M. Ceccarelli and S. M. Bezrukov, *Biophys. J.*, 2006, **90**, 1617–1617.
- 36 K. R. Mahendran, E. Hajjar, T. Mach, M. Lovelle, A. Kumar, I. Sousa, E. Spiga, H. Weingart, P. Gameiro, M. Winterhalter and M. Ceccarelli, *J. Phys. Chem. B*, 2010, **114**, 5170–5179.
- 37 M. Ceccarelli and P. Ruggerone, *Curr. Drug Targets*, 2008, **9**, 779–788.
- 38 E. Hajjar, A. Bessonov, A. Molitor, A. Kumar, K. R. Mahendran, M. Winterhalter, J.-M. Pages, P. Ruggerone and M. Ceccarelli, *Biochemistry*, 2010, **49**, 6928–6935.
- 39 P. Raj Singh, M. Ceccarelli, M. Lovelle, M. Winterhalter and K. R. Mahendran, *J. Phys. Chem. B*, 2012, **116**, 4433–4438.
- 40 P. Sampathkumar, F. Lu, X. Zhao, Z. Li, J. Gilmore, K. Bain, M. E. Rutter, T. Gheyi, K. D. Schwinn, J. B. Bonanno *et al.*, *Proteins: Struct., Funct., Bioinf.*, 2010, **78**, 3056–3062.
- 41 N. Eswar, B. Webb, M. A. Marti Renom, M. Madhusudhan, D. Eramian, M.-y. Shen, U. Pieper and A. Sali, *Current Protocols Bioinformatics*, 2006, 5.6.
- 42 W. F. Humphrey, A. Dalke and K. Schulten, *J. Mol. Graph.*, 1996, **14**, 33–38.
- 43 J. Gumbart, F. Khalili Araghi, M. Sotomayor and B. Roux, *Biochimica et Biophysica Acta (BBA)*, 2012, **1818**, 294–302.
- 44 J. C. Phillips, R. Braun, W. Wang, J. Gumbart, E. Tajkhorshid, E. Villa, C. Chipot, R. D. Skeel, L. Kale and K. Schulten, *J. Comput. Chem.*, 2005, **26**, 1781–1802.
- 45 A. MacKerell, D. Bashford, M. Bellott, R. Dunbrack, J. Evanseck, M. Field, S. Fischer, J. Gao, H. Guo, S. Ha, D. Joseph McCarthy, L. Kuchnir, K. Kuczera, F. Lau, C. Mattos, S. Michnick, T. Ngo, D. Nguyen, B. Prodhom, W. Reiher, B. Roux, M. Schlenkrich, J. Smith, R. Stote, J. Straub, M. Watanabe, J. Wiorkiewicz Kuczera, D. Yin and M. Karplus, *J. Phys. Chem. B*, 1998, **102**, 3586–3616.
- 46 T. Darden, D. York and L. Pedersen, *J. Chem. Phys.*, 1993, **98**, 10089–10092.
- 47 M. Tuckerman, B. Berne and G. Martyna, *J. Chem. Phys.*, 1992, **97**, 1990–2001.
- 48 W. Van Gunsteren and H. Berendsen, *Mol. Phys.*, 1977, **34**, 1311–1327.
- 49 Y. Liu and F. Zhu, *Biophys. J.*, 2013, **104**, 368–376.
- 50 N. Liu and A. H. Delcour, *Protein. Eng.*, 1998, **11**, 797–802.
- 51 E. L. Wu, P. J. Fleming, M. S. Yeom, G. Widmalm, J. B. Klauda, K. G. Fleming and W. Im, *Biophys. J.*, 2014, **106**, 2493–2502.